Analyst

ROYAL SOCIETY OF CHEMISTRY

PAPER

View Article Online
View Journal | View Issue

Check for updates

Cite this: *Analyst*, 2021, **146**, 2862

A carbon dot doped lanthanide coordination polymer nanocomposite as the ratiometric fluorescent probe for the sensitive detection of alkaline phosphatase activity†

Weidi Sun,[a] Xue Han,[b] Fengli Qu,[b] Rong-Mei Kong *[b] and Zilong Zhao *[a]

The development of sensitive methods for alkaline phosphatase (ALP) activity analysis is an important analytical topic. Based on the stimulus-responsive lanthanide coordination polymer, a simple ratiometric fluorescence sensing strategy was proposed to detect ALP activity. A carbon dot (CD) doped fluorescent supramolecular lanthanide coordination polymer (CDs@Tb-GMP) was prepared with Tb^{3+} and the ligand guanine single nucleotide (GMP). To construct a ratiometric fluorescence biosensor, the fluorescence of Tb-GMP was used as a response signal, and the fluorescence of CDs was used as a reference signal due to its good stability. When excited at 290 nm, the polymer network Tb-GMP emits characteristic fluorescence at 545 nm, while the CDs encapsulated in the polymer network emit fluorescence at 370 nm. After adding ALP to the system, the substrate GMP can be hydrolyzed by ALP, resulting in the destruction of the polymer network. Accordingly, the fluorescence of Tb-GMP significantly decreased, while the fluorescence of CDs slightly increased due to their release from the polymer network. By comparing the relationship between the fluorescence intensity ratio of the two signals and the concentration of ALP, sensitive detection of ALP could be achieved with the linear range from 0.5 to 80 U L^{-1} and a detection limit of 0.13 U L^{-1}. Furthermore, the proposed ratiometric sensing system was applied to the detection of ALP in human serum samples with desirable results, indicating potential application in clinical diagnosis.

Received 3rd February 2021,
Accepted 1st April 2021

DOI: 10.1039/d1an00218j

rsc.li/analyst

Published on 01 April 2021. Downloaded on 5/15/2021 10:45:07 AM.

1. Introduction

Alkaline phosphatase (ALP) is widely distributed in the animal and microbial community and can non-specifically catalyze the hydrolysis of almost all phosphate monoesters, thereby participating in various biological processes.[1] In addition, this commonly used hydrolase is also involved in signal transduction and the regulation of intracellular cell growth and apoptosis processes.[2,3] ALP activity in serum is often used as an important indicator for clinical diagnosis and treatment of human diseases.[4–7] Therefore, accurate and sensitive assessment of ALP activity is of great significance for understanding the molecular mechanism of phosphate hydrolysis, biochemical analysis, diagnosis and treatment of clinical diseases. Many methods have been developed for ALP activity detection, such as electrochemiluminescence,[8] surface enhanced Raman scattering,[9] colorimetry,[10–12] fluorescence[13–16] and electrochemistry.[17–20] The detection principle is mainly based on the ability of ALP to remove phosphate groups from various substrates and obtain signal readings. Among the various methods proposed, each method has its own advantages and provides different opinions on ALP detection. However, most of them usually require complicated analytical processing and instrument operation as well as unsatisfactory sensitivity, which are still far from practical application to biological systems.

Fluorescence technology is very attractive in this respect because of its inherent advantages such as high sensitivity, easy operation and availability in living organisms.[21,22] So far, a variety of fluorescence analysis methods for ALP using organic dyes,[23–25] conjugated polyelectrolytes,[26,27] quantum dots[28,29] or metal nanoclusters[16] as fluorescent materials have been reported. However, these methods are usually plagued with disadvantages, such as poor water solubility and light stability of organic dyes, small Stokes shift, complex synthesis process of conjugated polyelectrolytes, cytotoxicity of quantum dots, high cost of noble metal nanoclusters and poor stability in aqueous systems, which limit their further application.

[a]*State Key Laboratory of Chemo/Biosensing and Chemometrics, College of Chemistry and Chemical Engineering, Hunan University, Changsha, 410082, P. R. China. E-mail: kongrongmei@126.com, zlzhao@hnu.edu.cn; Tel: (+86) 537-4456301; Fax: (+86) 537-4456301*

[b]*College of Chemistry and Chemical Engineering, Qufu Normal University, Qufu, Shandong 273165, P. R. China*

†Electronic supplementary information (ESI) available. See DOI: 10.1039/d1an00218j

This journal is © The Royal Society of Chemistry 2021

Published on 01 April 2021. Downloaded on 5/15/2021 10:45:07 AM.

Therefore, it is still highly desirable to develop new fluorescent materials with high selectivity, high light stability and low toxicity for the ALP activity detection.

In recent years, lanthanide coordination polymers (LnCPs), which are self-assembled by lanthanide ions (Ln^{3+}) and organic ligands, have attracted a wide range of interest due to their highly controllable, diverse structures, excellent encapsulation ability and inherent biocompatibility.[30–32] Due to the f-f electronic transition of Ln^{3+}, LnCPs exhibit several unique optical properties, such as large Stokes shift, narrow emission peak and long fluorescence lifetime.[33] Therefore, the fluorescence measurement based on LnCPs has more obvious advantages than the traditional fluorescence methods in eliminating background interference and detecting scattered fluorescence through time delay. Over the last two decades, fluorescent probes based on LnCPs have shown a wide range of applications and have been used to detect metal ions,[34] anions,[35] and various biomolecules.[36,37] These studies have made great contributions to the development of fluorescent sensors based on LnCPs. However, most of these sensors rely on a single response or intensity changing fluorescent signal, which are easily affected by various factors, including the fluctuation of light source intensity and environmental impact, such as pH, medium polarity and photobleaching.[38,39] Therefore, the resultant poor sensitivity and accuracy limit their further practical application. The ratiometric fluorescence method measures the changes of the fluorescence intensity ratio at two different wavelengths to achieve the purpose of target analysis. As a consequence, the ratiometric fluorescence method can eliminate the environmental fluctuations, overcome the problems inherent in the above existing methods, and realize reliable detection of targets of interest. In addition, high sensitivity can be achieved by acquiring the amplified signals of two channels simultaneously.[40,41]

Guanine mononucleotide (GMP) is one of the nucleotides constituting nucleic acid, and its nucleobase part and phosphate group can be used as the bidentate ligand of Tb^{3+}.[42] The strong green fluorescence can be observed from the Tb-GMP chelate, which is due to the sensitization of the guanine part of GMP and the improvement of the energy transfer efficiency of GMP to Tb^{3+} caused by the phosphate group of GMP.[43] In this work, we develop a ratiometric fluorescent probe based on LnCPs doped with carbon dots (CDs@Tb-GMP) for ALP detection. As shown in Scheme 1, in this probe, Tb-GMP was selected as the recognition and signal response group for ALP detection, and CDs were selected as the signal reference group. The as-prepared CDs have a wide absorption band that can match the excitation wavelength of Tb-GMP; therefore, the CDs@Tb-GMP can be excited by a single wavelength while emitting the blue fluorescence of CDs and green fluorescence of Tb-GMP at the same time, respectively. In the presence of ALP, the phosphate group in GMP ligands can be hydrolyzed by ALP, resulting in the destruction of the Tb-GMP network, and the characteristic emission intensity of Tb-GMP at 545 nm is significantly reduced. Meanwhile, due to the hydrolysis of the polymer network, CDs are released into the solution, resulting in a slight increase in the fluorescence of CDs at 370 nm. Therefore, by comparing the relationship between the fluorescence intensity ratio of F_{370}/F_{545} and the concentration of ALP, sensitive detection of ALP can be achieved.

2. Experimental section

2.1. Reagents and apparatus

Alkaline phosphatase (ALP), guanosine-5-monophosphate disodium salt (GMP), terbium nitrate ($Tb(NO_3)_3$), trypsin, and horseradish peroxidasen (HRP) were purchased from Sigma-

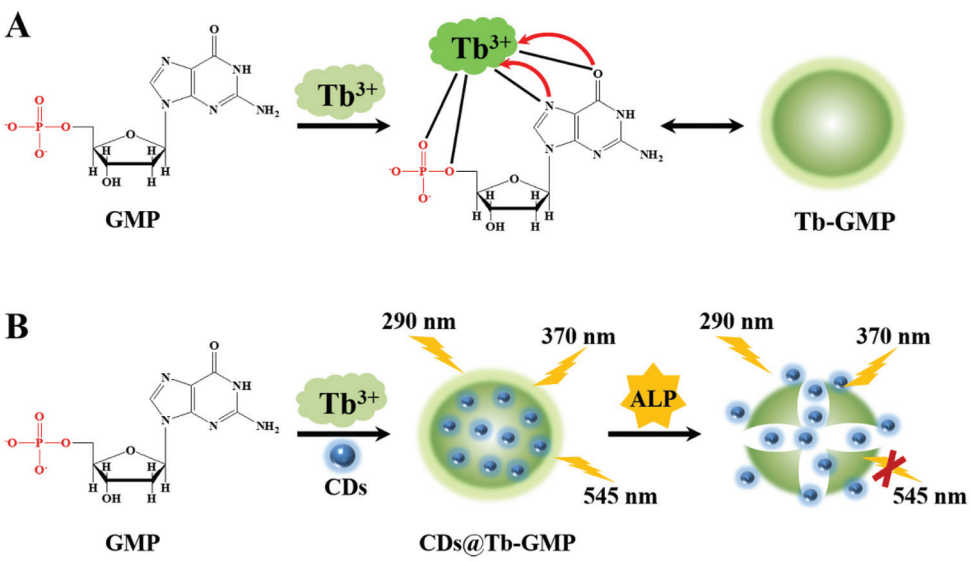

Scheme 1 Schematic illustration of the interaction between Tb^{3+} and GMP (A), and the CDs@Tb-GMP probe for ratiometric fluorescence detection of ALP activity (B).

Published on 01 April 2021. Downloaded on 5/15/2021 10:45:07 AM.

Aldrich Co. LLC. (St Louis Missouri, USA). Glutathione (GSH), bovine serum albumin (BSA), uric acid (UA), heparin, cysteine (Cys), glycine (Gly), phenylalanine (L-Phe) and hydrogen peroxide (H_2O_2) were obtained from Aladdin Industrial Inc. (Shanghai, China). Metal salts including NaCl, $FeCl_2$, $FeCl_3$, $CaCl_2$, $MgCl_2$ and $ZnCl_2$ were obtained from Sinopharm Chemical Reagent Co. Ltd (Shanghai, China). 0.1 M HEPES buffer solution (pH 7.4) was used for the preparation of Tb-GMP and CDs@Tb-GMP. 50 mM Tris-HCl buffer solution (Tris-HCl, 5 mM $MgCl_2$, pH 8.0) was used for controlling the pH of the detection system. The ultra-pure water (resistivity > 18 MΩ cm) used for the preparation of aqueous solutions was produced using a Millipore system.

The morphology and size characterization of the as-prepared materials were performed using a scanning electron microscope (SEM, JSM-6700F, Japan) and a transmission electron microscope (TEM, JEM-2100PLUS, Japan). The UV–vis spectra were recorded by using a Cary-300 UV-vis spectrophotometer (Varian, USA). The fluorescence spectra were recorded using an F-7000 spectrometer (Hitachi, Japan) with an excitation wavelength at 290 nm, both excitation and emission slit widths of 10.0 nm and a PMT detector voltage of 700 V. X-ray photoelectron spectroscopy (XPS) was conducted on an ESCALAB 250Xi spectrometer (Thermo Fisher, USA). Fourier transform infrared (FT-IR) spectra were recorded on a Nicolet iS5 Fourier transform infrared spectrometer (Thermo Fisher, USA).

2.2. Preparation of CDs

According to the protocol reported in the literature, blue light-emitting CDs were prepared by the microwave method.[44] Briefly, 0.3 g of Gly and 1 g of urea were dissolved in ultrapure water, and then the solution was heated in a microwave oven for 4 min. The obtained black solid powder was dissolved with 10 mL of ultrapure water. The supernatant was collected by centrifugation at 12000 rpm for 5 min, and then the supernatant was dialyzed using a dialysis membrane for 48 h to remove excess precursors and small molecules. The synthesized CDs were stored in a refrigerator at 4 °C.

2.3. Preparation of Tb-GMP and CDs@Tb-GMP

The Tb-GMP nanocomposite was synthesized according to the literature reported method.[43] Firstly, the aqueous solution of $Tb(NO_3)_3{\cdot}6H_2O$ (8 mM, 1 mL) was mixed with GMP (8 mM, prepared with HEPES buffer solution) to form a white precipitate at room temperature. The precipitate was centrifugally washed three times (8000 rpm, 5 min) and then dissolved in 2 mL of ultra-pure water. The prepared materials were stored in a refrigerator at 4 °C.

The synthesis of CDs@Tb-GMP nanocomposites was carried out according to the following steps: the GMP (8 mM, prepared with HEPES buffer solution) was added into 1 mL of CDs which diluted 5 times, and the mixture was incubated at 25 °C for 30 min. Then, the aqueous solution of Tb $(NO_3)_3{\cdot}6H_2O$ (8 mM, 1 mL) was added into GMP-CDs (1 mL) to obtain white precipitate. The precipitates were washed three times *via* centrifugation (8000 rpm, 5 min), and redispersed in 2 mL of ultra-pure water. The prepared materials were stored in a refrigerator at 4 °C.

2.4. Fluorescence detection of ALP

The ratio fluorescence measurement of ALP activity was performed according to the following procedure. After adding 40 μL of ALP with different concentrations into 40 μL of CDs@Tb-GMP solution, the Tris-HCl buffer was used to maintain the reaction system at 200 μL, and then incubated in a 37 °C water bath for 30 min. Then, the fluorescence spectra of the solutions were recorded at the excitation wavelength of 290 nm. For detecting the ALP in real complex samples, experiments were conducted in diluted human serum samples from healthy volunteers. Informed consent was obtained from human participants of this study. The serum sample experiments were approved by the Ethical Committee of Qufu Normal University and performed according to its Guidelines.

3. Results and discussion

3.1 The feasibility of the sensing system

Based on the stimulus-responsive LnCPs, a simple and novel ALP active fluorescence sensing strategy was proposed. The supramolecular LnCPs were constructed using Tb^{3+} as the metal ion and GMP as the ligand. Due to the unique ability of self-association, GMP was selected as a ligand model to form ordered nanostructures. GMP can form large chelates through the coordination of the guanine moiety and N and O atoms in the phosphate group with Tb^{3+}, and the resulting supramolecular coordination polymer network has adaptive inclusion properties.[42,45] Due to the energy transfer from guanine to the emitted D4 state of Tb^{3+}, the Tb-GMP network emits fluorescence at 490, 545, 585 and 620 nm (Fig. 1, curve b). By simply mixing GMP, Tb^{3+} and blue-emitting CDs (Fig. 1, curve a), CDs can be encapsulated as guest molecules inside the

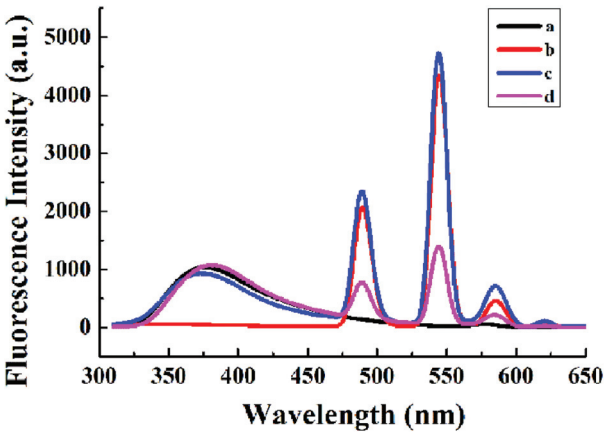

Fig. 1 Fluorescence emission spectra of (a) CDs, (b) Tb-GMP, (c) CDs@Tb-GMP and (d) CDs@Tb-GMP + 60 U L^{-1} ALP. The volumes of CDs (diluted 5 times), Tb-GMP, and CDs@Tb-GMP used in this experimental section are all 50 μL, respectively. The total volume of the detection solution is 200 μL.

This journal is © The Royal Society of Chemistry 2021

Published on 01 April 2021. Downloaded on 5/15/2021 10:45:07 AM.

coordination polymer network to form CDs@Tb-GMP nanocomposites. In order to verify the encapsulation of CDs in the Tb-GMP network, the fluorescence spectra of the CDs@Tb-GMP nanomaterials were recorded. As shown in Fig. 1 (curve c), the characteristic emission peaks of CDs at 370 nm and Tb-GMP at 490, 545, 585 and 620 nm were observed, indicating the successful encapsulation of CDs. When ALP was added, which can catalyze the removal of the phosphate group from the GMP ligand, the Tb-GMP polymer network was destroyed, resulting in a significant decrease in the characteristic peaks of Tb-GMP, while the fluorescence intensity of CDs slightly increased due to their release from the network (Fig. 1, curve d). Therefore, the fluorescence of CDs was selected as the reference signal, and the fluorescence of Tb-GMP was used as the response signal. The change in fluorescence intensity ratio of F_{370}/F_{545} with ALP concentration was recorded to realize the sensitive detection of ALP activity.

3.2 Characterization of Tb-GMP and CDs@Tb-GMP

The morphologies of the as-synthesized CDs, Tb-GMP and CDs@Tb-GMP nanomaterials were characterized by SEM and TEM. As shown in Fig. S1A,† the TEM image indicates that the synthesized CDs are well dispersed with uniform particle size. The corresponding particle size distribution histograms indicated that the average diameter is about 2.9 nm (Fig. S1B†). As shown in Fig. 2B and D, the CDs@Tb-GMP nanoparticles were colloidal spheres with a diameter range of about 40–50 nm, which are similar to the morphology and size of the Tb-GMP network polymer (Fig. 2A and C). The results indicate that the encapsulation of CDs does not change the structure or morphology of the Tb-GMP network.

The assembly mechanism of the coordination polymer was further explored by FT-IR (Fig. 3A). The absorption peaks at 1630 and 1489 cm^{-1} were attributed to the C═O and N–C stretching vibration bands of the GMP guanosine part, and the peaks at 1073 and 980 cm^{-1} belonged to the antisymmetric and symmetric vibration bands of the GMP phosphoric acid part. When the Tb^{3+} ion was added, the GMP interacted with Tb^{3+} to form Tb-GMP nanocomplexes. The absorption wave numbers of GMP were shifted to 1637, 1467, 1112 and 994 cm^{-1}, indicating that both the phosphate group and guanosine unit of GMP play important role in the coordination bond.[46,47] For CDs@Tb-GMP, compared with Tb-GMP, no significant wave number shifts of the corresponding peaks were observed, indicating that CDs are mainly confined within the Tb-GMP polymer network and have no significant effect on the coordination between Tb^{3+} and GMP.

Fig. 3B shows the XPS spectra of GMP, Tb-GMP and CDs@Tb-GMP. The peaks of GMP at 130.6, 285.0, 399.2, and 531.8 eV were attributed to P 2p, C 1s, N 1s, and O 1s, respectively. After binding with Tb^{3+} to form Tb-GMP, the peaks of N 1s and O 1s of GMP changed to 398.8 eV and 530.8 eV, respectively, indicating that the coordination of Tb^{3+} with GMP is through the synergistic action of N and O. In addition, the appearance of the peaks at 145.9 eV and 1242.1 eV, which belonged to Tb 4d and Tb 3d, respectively, confirmed the successful synthesis of Tb-GMP. After the CDs were encapsulated into the Tb-GMP polymer network, the peaks did not change

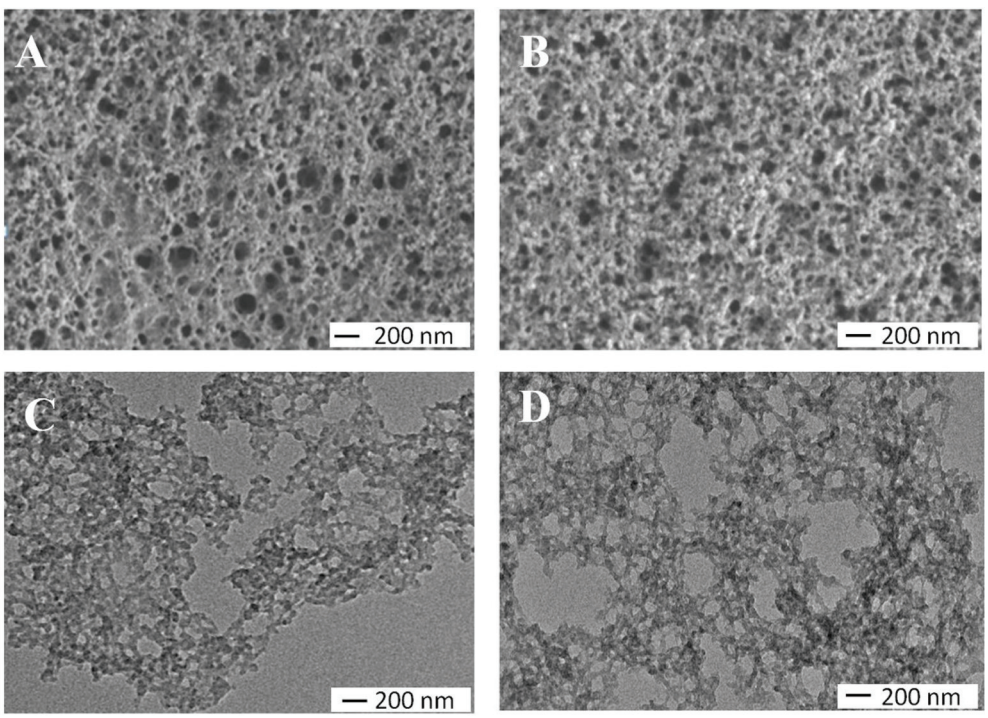

Fig. 2 SEM images of (A) Tb-GMP and (B) CDs@Tb-GMP and TEM images of (C) Tb-GMP and (D) CDs@Tb-GMP.

Published on 01 April 2021. Downloaded on 5/15/2021 10:45:07 AM.

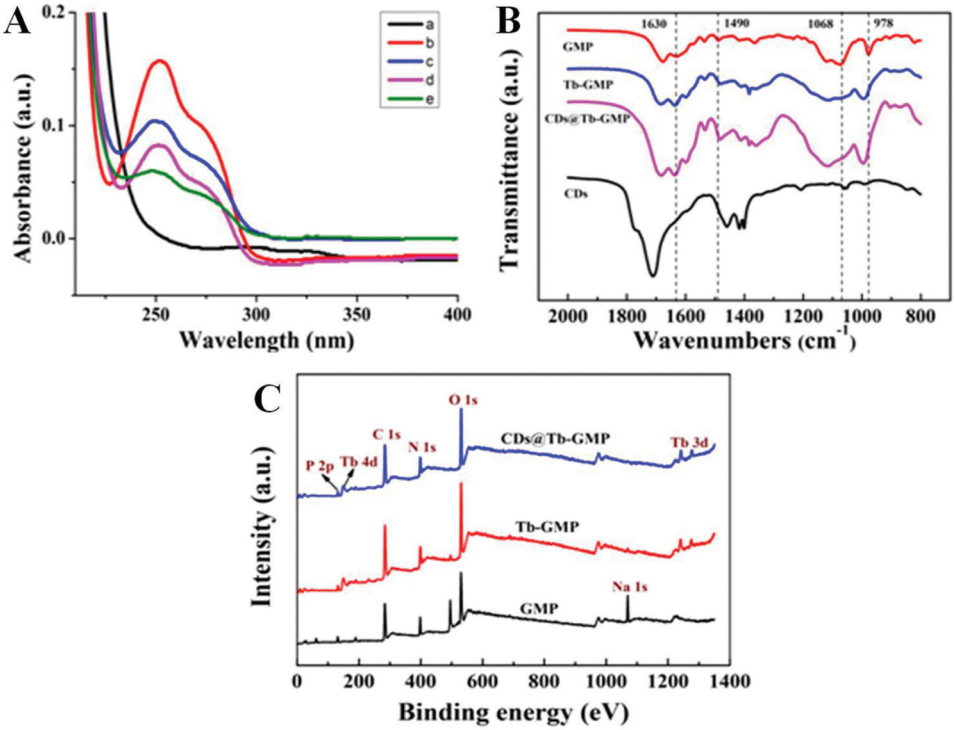

Fig. 3 (A) FT-IR spectra of GMP, Tb-GMP, CDs@Tb-GMP and CDs. (B) XPS spectra of CDs@Tb-GMP, Tb-GMP and GMP. (C) UV-Vis absorption spectra of (a) CDs, (b) GMP, (c) Tb-GMP, (d) CDs@Tb-GMP and (e) CDs@Tb-GMP + ALP.

significantly, indicating that the encapsulation of CDs has little effect on the coordination between Tb-GMP.

In order to verify the incorporation of CDs into the Tb-GMP network polymer and the disintegration of the Tb-GMP network triggered by ALP, the UV-vis absorption spectra were investigated under different conditions. As shown in Fig. 3C, the CDs presented an absorption at 300 nm due to n-π* transition (curve a), and GMP in aqueous solution presented two characteristic absorption peaks at 252 and 276 nm due to the two π–π* transitions of guanine (curve b).[46,47] After the Tb^{3+} ion was complexed with GMP, the absorbance of the Tb-GMP network polymer was decreased (curve c). For the CDs@Tb-GMP network polymer, the absorbance at 300 nm is greatly weakened, indicating that CDs have been successfully encapsulated in the Tb-GMP polymer network, thereby shielding the absorption of CDs (curve d). In the presence of ALP, the absorbance of Tb-GMP decreased again, verifying the hydrolysis of GMP by ALP which resulted in the disintegration of the Tb-GMP polymer network (curve e).

3.3 Optimization of the experimental conditions

To obtain a high fluorescence sensing performance of the proposed method for ALP detection, the main experimental factors were investigated. First, the effect of pH on the probe fluorescence intensity ratio F_{370}/F_{545} was studied (Fig. 4A). The experimental result shows that the probe has the largest fluorescence intensity ratio at pH 8.0 for the detection of ALP, thus pH 8.0 was selected as the optimal pH for the reaction. In addition, since Mg^{2+} can catalyze the hydrolysis of phosphate groups by ALP, the effect of the Mg^{2+} concentration in Tris-HCl buffer solution on the detection of ALP was studied. As shown in Fig. 4B, the concentration of Mg^{2+} at 10 mM is appropriate for the response to ALP that with the highest ratio intensity of F_{370}/F_{545}. Finally, the effect of the incubation time of ALP on the fluorescence intensity ratio of the system was studied. As shown in Fig. 4C, after the addition of ALP, the fluorescence intensity ratio of F_{370}/F_{545} gradually increased with the incubation time and reached a relatively stable value at 30 min. Therefore, 30 min was chosen as the appropriate incubation time for subsequent experiments.

3.4 The analysis performance for ALP detection

To investigate the analysis performance of the CDs@Tb-GMP probe, different concentrations of ALP was incubated with CDs@Tb-GMP nanocomposite solution under optimal experimental conditions. Fig. 5A depicts the changes of the fluorescence spectra of CDs@Tb-GMP after incubation with ALP. With an increase in ALP concentration, the fluorescence of CDs at 370 nm slightly increased, while the fluorescence of Tb-GMP at 545 nm significantly decreased. The fluorescence intensity of CDs increased with an increase in ALP concentration, which might be attributed to the following reason. When the CDs were wrapped in the polymer network, the excitation light was partially blocked by the GMP shell, resulting

 This journal is © The Royal Society of Chemistry 2021

Published on 01 April 2021. Downloaded on 5/15/2021 10:45:07 AM.

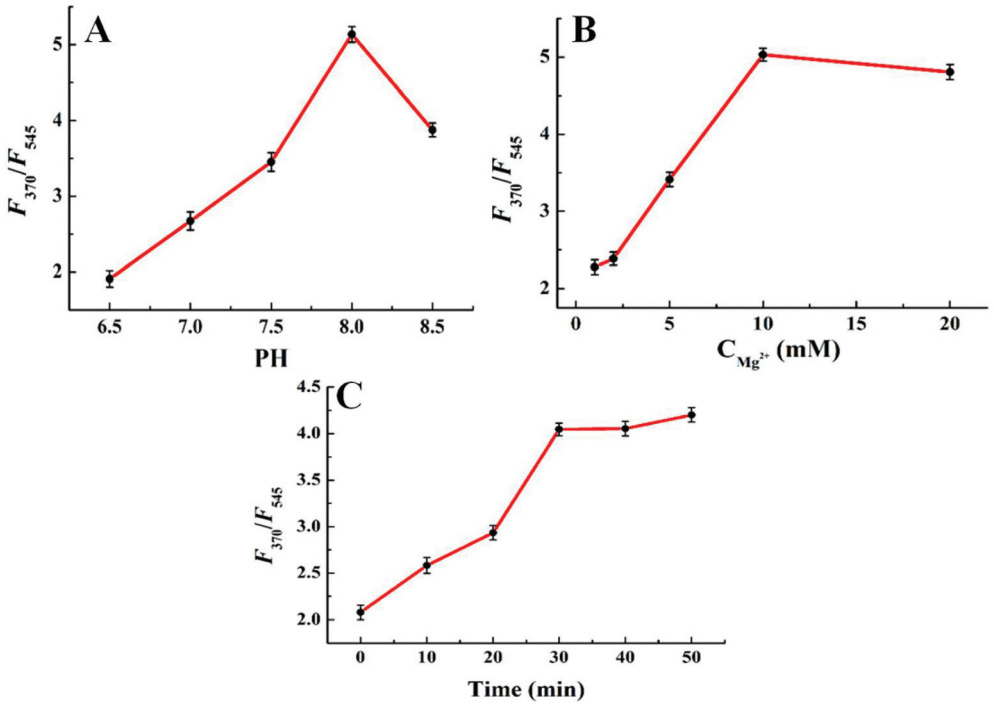

Fig. 4 (A) The effects of the concentrations of Mg^{2+} on the fluorescence intensity ratio (F_{370}/F_{545}). (B) The effect of the pH on the fluorescence intensity ratio (F_{370}/F_{545}). (C) The effect of the enzymatic reaction time of ALP for hydrolysis of GMP on the fluorescence intensity ratio (F_{370}/F_{545}).

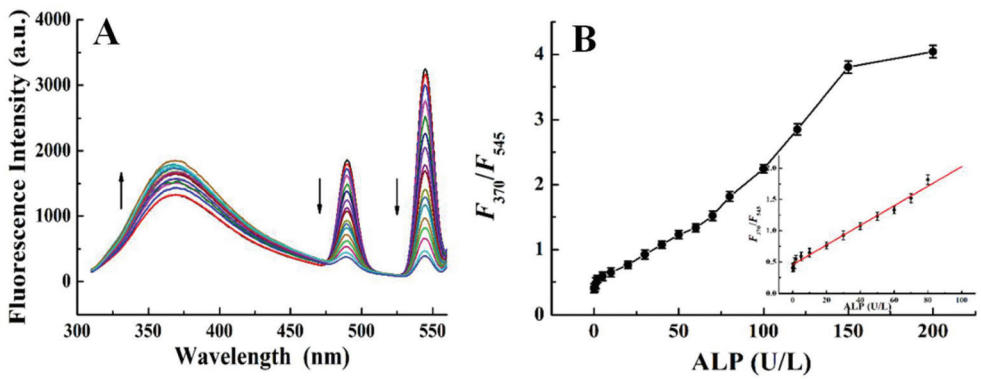

Fig. 5 (A) The fluorescence spectra of the sensing system in the presence of different concentrations of ALP. (B) Linear relationship between ALP concentration and fluorescence intensity ratio (F_{370}/F_{545}).

in the relatively low fluorescence intensity of CDs. After the disruption of the polymer network by ALP, the CDs were released, thus resulting in the slight recovery of the fluorescence. These results show that CDs@Tb-GMP is suitable as a ratiometric probe for detecting ALP. Using the fluorescence of Tb-GMP as the response signal, and the fluorescence of CDs as the reference signal, the ratiometric signal output of the probe endowed it with a built-in correction function to avoid the environmental impact on the analysis. As shown in Fig. 5B, when the concentration of ALP increased from 0 U L^{-1} to 200 U L^{-1}, the emission intensity ratio of F_{370}/F_{545} gradually increased. The method had a good linear relationship between fluorescence intensity ratio (F_{370}/F_{545}) and the concentration of ALP in the range from 0.5 to 80 U L^{-1}, with the regression equation of F_{370}/F_{545} = 0.45923 + 0.01569C_{ALP} (U L^{-1}), R^2 = 0.991. The detection limit for ALP is calculated to be 0.13 U L^{-1} based on 3σ/slope. Compared with the previously reported ALP detection method, this probe shows better or comparable sensitivity (Table S1†). In addition, the detection process of the proposed probe for ALP is simple and fast, and the synthesis of CDs@Tb-GMP nanocomposites is convenient.

Published on 01 April 2021. Downloaded on 5/15/2021 10:45:07 AM.

3.5 Selectivity study for ALP detection

To evaluate the specificity of the developed sensing system for ALP, the influence of various interfering substances, including common metals (Na^+, Zn^{2+}, Mg^{2+}, Ca^{2+}, Fe^{3+}, and Fe^{2+}), amino acids (Cys, Gly, and L-Phe,), redox chemicals (GSH, UA, and H_2O_2), and other nonspecific substances (BSA, HRP, trypsin and heparin) were investigated under the same conditions. Among them, the concentration of ALP was 50 U L^{-1}, the concentration of metal ions, amino acids and redox chemicals were all 100 μM, the concentration of BSA was 0.2 mg mL^{-1}, and the concentrations of enzymes including HRP, pepsin and heparin are both 100 U L^{-1}. As shown in Fig. 6, the value of F_{370}/F_{545} increased significantly after ALP was added into the system. However, the value of F_{370}/F_{545} remained unchanged even when the concentration of these substances was 10 times higher than that of ALP. The results indicate that the proposed ratiometric fluorescent probe in this work has high selectivity for the detection of ALP.

3.6 Detection of ALP activity in human serum samples

To further estimate the practical application of the proposed method, the measurement of spiked ALP in diluted human serum was carried out. Taking into the account the ALP level in healthy human serum and the linear range of our method, the serum samples were diluted 50-fold before being tested. As shown in Table 1, the recoveries were in the range from 96.5% to 105.4% with the relative standard deviations (RSD) lower than 4.5%. These results indicate the potential of this method in complicated biological environments.

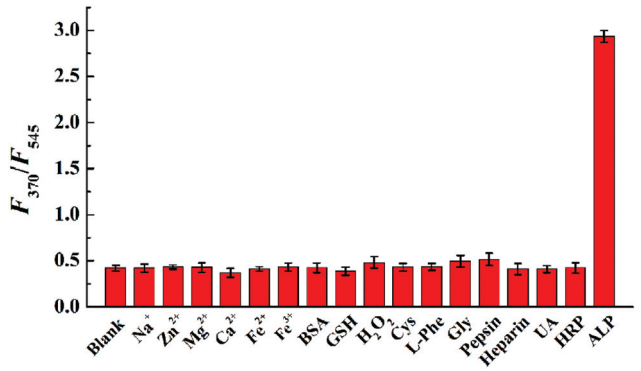

Fig. 6 Selectivity of the sensing system for ALP detection.

Table 1 Recovery of ALP from human serum samples using the standard addition method

Sample	Found (U L^{-1})	Added (U L^{-1})	Total found (U L^{-1})	Recovery (%)	RSD (n = 3, %)
Sample 1		2.0	2.09	104.5	3.6
	0.0	5.0	4.87	97.4	4.1
		10.0	10.36	103.6	4.5
Sample 1		2.0	2.33	96.5	3.8
	0.4	5.0	5.67	105.4	4.3
		10.0	10.88	104.8	3.7

4. Conclusions

In summary, a kind of carbon dot doped lanthanide coordination polymer (CDs@Tb-GMP) nanocomposite has been successfully prepared by simple mixing and employed as a ratiometric probe for sensitive detection of ALP activity. The CDs@Tb-GMP nanocomposites can emit the fluorescence at 370 nm of CDs and the fluorescence at 545 nm of Tb simultaneously when excited at 290 nm. Tb-GMP in the CDs@Tb-GMP nanocomposite acted as the recognition and signal response group and CDs acted as the signal reference group, which endowed the probe with a built-in correction function to avoid environmental influences. After adding the analyte ALP to the system, the fluorescence of Tb-GMP in the CDs@Tb-GMP nanomaterials significantly decreased due to the hydrolysis of the Tb-GMP polymer network, while the fluorescence of CDs only slightly increased due to their release from the polymer network. By comparing the relationship between the fluorescence intensity ratio F_{370}/F_{545} of two signals and the concentration of ALP, the sensitive detection of ALP was realized with a detection limit of 0.13 U L^{-1}. More importantly, the ratiometric fluorescent probe could be used to detect ALP under physiological conditions. Therefore, the proposed method has great potential for evaluating ALP in clinical analysis.

Conflicts of interest

There are no conflicts to declare.

Acknowledgements

This work was supported by the National Natural Science Foundation of China (No. 21775089, 22074080, and 21974040), the Natural Science Foundation Projects of Shandong Province (ZR2017QB008 and ZR2020KB020), the Changjiang Scholar Program of the Ministry of Education of China, and the Taishan Scholar Program of Shandong Province (tsqn201909106).

References

1 D. W. Moss, Perspectives in alkaline phosphatase research, *Clin. Chem.*, 1992, **38**, 2486–2492.
2 S. G. Julien, N. Dubé, S. Hardy and M. L. Tremblay, Inside the human cancer tyrosine phosphatome, *Nat. Rev. Cancer*, 2011, **11**, 35–49.
3 L. N. Johnson and R. J. Lewis, Structural basis for control by phosphorylation, *Chem. Rev.*, 2001, **101**, 2209–2242.

This journal is © The Royal Society of Chemistry 2021

Published on 01 April 2021. Downloaded on 5/15/2021 10:45:07 AM.

4 A. L. Wiedemann, S. C. Charney, A. M. Barger, D. J. Schaeffer and B. E. Kitchell, Assessment of corticosteroid-induced alkaline phosphatase as a prognostic indicator in canine lymphoma, *J. Small Anim. Pract.*, 2005, **46**, 185–190.

5 J. Sato, K. Okada, S. Fukuda, R. Sato, J. Yasuda and Y. Naito, Serum activities of tartrate-resistant acid phosphatase and bone specific alkaline phosphatase as indices of bone metabolism in the cow, *J. Vet. Med. Sci.*, 2002, **64**, 653–655.

6 C. Jin, J. X. He, J. M. Zou, W. J. Xuan, T. Fu, R. W. Wang and W. H. Tan, Phosphorylated lipid-conjugated oligonucleotide selectively anchors on cell membranes with high alkaline phosphatase expression, *Nat. Commun.*, 2019, **10**, 2704.

7 A. L. Brichacek and C. M. Brown, Alkaline phosphatase: a potential biomarker for stroke and implications for treatment, *Metab. Brain Dis.*, 2019, **34**, 3–19.

8 A. N. Ďıaz, F. Ga Sánchez, M. C. Ramos and M. C. Torijas, Horseradish peroxidase solgel immobilized for chemiluminescence measurements of alkaline-phosphatase activity, *Sens. Actuators, B*, 2002, **82**, 176–179.

9 Y. Zeng, J. Q. Ren, S. K. Wang, J. M. Mai, B. Qu, Y. Zhang, A. G. Shen and J. M. Hu, Rapid and reliable detection of alkaline phosphatase by a hot spots amplification strategy based on well-controlled assembly on single nanoparticle, *ACS Appl. Mater. Interfaces*, 2017, **9**, 29547–29553.

10 H. Song, K. Ye, Y. Peng, L. Wang and X. Niu, Facile colorimetric detection of alkaline phosphatase activity based on the target-induced valence state regulation of oxidase-mimicking Ce-based nanorods, *J. Mater. Chem. B*, 2019, **7**, 5834–5841.

11 H. Wei, C. Chen, B. Han and E. Wang, Enzyme colorimetric assay using unmodified silver nanoparticles, *Anal. Chem.*, 2008, **80**, 7051–7055.

12 Y. Liu and K. S. Schanze, Conjugated polyelectrolyte-based real-time fluorescence assay for alkaline phosphatase with pyrophosphate as substrate, *Anal. Chem.*, 2008, **80**, 8605–8612.

13 Z. Lv, Q. Wang and M. Yang, DNAzyme-Au nanoprobe coupled with graphene-oxide-loaded hybridization chain reaction signal amplification for fluorometric determination of alkaline phosphatase, *Microchim. Acta*, 2021, **7**, 188.

14 R. M. Kong, T. Fu, N. N. Sun, F. L. Qu, S. F. Zhang and X. B. Zhang, Pyrophosphate-regulated Zn^{2+}-dependent DNAzyme activity: An amplified fluorescence sensing strategy for alkaline phosphatase, *Biosens. Bioelectron.*, 2013, **50**, 351–355.

15 R. Freeman, T. Finder, R. Gill and I. Willner, Probing protein kinase (CK2) and alkaline phosphatase with CdSe/ZnS quantum dots, *Nano Lett.*, 2010, **10**, 2192–2196.

16 L. L. Zhang, J. J. Zhao, M. Duan, H. Zhang, J. H. Jiang and R. Q. Yu, Inhibition of dsDNA-templated copper nanoparticles by pyrophosphate as a label-free fluorescent strategy for alkaline phosphatase assay, *Anal. Chem.*, 2013, **85**, 3797–3801.

17 B. Kazakevičienė, G. Valinčius, M. Kažemėkaitė and V. Razumas, Self-assembled redox system for bioelectrocatalytic assay of l-ascorbylphosphate and alkaline phosphatase activity, *Electroanalysis*, 2008, **20**, 2235–2240.

18 T. Murata, T. Yasukawa, H. Shiku and T. Matsue, Electrochemical single-cell geneexpression assay combining dielectrophoretic manipulation with secreted alkaline phosphatase reporter system, *Biosens. Bioelectron.*, 2009, **25**, 913–919.

19 P. Miao, L. Ning, X. Li, Y. Shu and G. Li, An electrochemical alkaline phosphatase biosensor fabricated with two DNA probes coupled with λ exonuclease, *Biosens. Bioelectron.*, 2011, **27**, 178–182.

20 K. Ino, Y. Kanno, T. Arai, K. Y. Inoue, Y. Takahashi, H. Shiku and T. Matsue, Novel electrochemical methodology for activity estimation of alkaline phosphatase based on solubility difference, *Anal. Chem.*, 2012, **84**, 7593–7598.

21 L. Jia, J. P. Xu, D. Li, S. P. Pang, Y. Fang, Z. G. Song and J. Ji, Fluorescence detection of alkaline phosphatase activity with β-cyclodextrin-modified quantum dots, *Chem. Commun.*, 2010, **46**, 7166–7168.

22 N. Malashikhina, G. Garai-Ibabe and V. Pavlov, Unconventional application of conventional enzymatic substrate: First fluorogenic immunoassay based on enzymatic formation of quantum dots, *Anal. Chem.*, 2013, **85**, 6866–6870.

23 S. J. Li, C. Y. Li, Y. F. Li, J. Fei, P. Wu, B. Yang, J. Ou-Yang and S. X. Nie, Facile and sensitive near-infrared fluorescence probe for the detection of endogenous alkaline phosphatase activity in vivo, *Anal. Chem.*, 2017, **89**, 6854–6860.

24 J. Liang, R. T. K. Kwok, H. Shi, B. Z. Tang and B. Liu, Fluorescent light-up probe with aggregation-induced emission characteristics for alkaline phosphatase sensing and activity study, *ACS Appl. Mater. Interfaces*, 2013, **5**, 8784–8789.

25 X. Gu, G. Zhang, Z. Wang, W. Liu, L. Xiao and D. Zhang, A new fluorometric turn-on assay for alkaline phosphatase and inhibitor screening based on aggregation and deaggregation of tetraphenylethylene molecules, *Analyst*, 2013, **138**, 2427–2431.

26 Y. Li, X. Wang and X. Su, A label-free conjugated polymer-based fluorescence assay for the determination of adenosine triphosphate and alkaline phosphatase, *New J. Chem.*, 2014, **38**, 4574–4579.

27 A. H. Malik, S. Hussain, A. S. Tanwar, S. Layek, V. Trivedi and P. K. Iyer, An anionic conjugated polymer as a multiaction sensor for the sensitive detection of Cu^{2+} and PPi, real-time ALP assaying and cell imaging, *Analyst*, 2015, **140**, 4388–4392.

28 S. Liu, S. Pang, W. Na and X. Su, Near-infrared fluorescence probe for the determination of alkaline phosphatase, *Biosens. Bioelectron.*, 2014, **55**, 249–254.

Published on 01 April 2021. Downloaded on 5/15/2021 10:45:07 AM.

29 S. Liu, X. Wang, S. Pang, W. Na, X. Yan and X. Su, Fluorescence detection of adenosine-5-triphosphate and alkaline phosphatase based on the generation of CdS quantum dots, *Anal. Chim. Acta*, 2014, **827**, 103–110.
30 F. Y. Wang, X. Hu, J. Hu, Q. Q. Peng, B. Z. Zheng, J. Du and D. Xiao, Fluorescence assay for alkaline phosphatase activity based on energy transfer from terbium to europium in lanthanide coordination polymer nanoparticles, *J. Mater. Chem. B*, 2018, **6**, 6008–6015.
31 Y. J. Tong, L. D. Yu, L. L. Wu, S. P. Cao, R. P. Liang, L. Zhang, X. H. Xia and J. D. Qiu, Aggregation-induced emission of luminol: a novel strategy for fluorescence ratiometric detection of ALP and As(v) with high sensitivity and selectivity, *Chem. Commun.*, 2018, **54**, 7487–7490.
32 Q. X. Wang, S. F. Xue, Z. H. Chen, S. H. Ma, S. Q. Zhang, G. Y. Shi and M. Zhang, Dual lanthanide-doped complexes: the development of a time-resolved ratiometric fluorescent probe for anthrax biomarker and a paper-based visual sensor, *Biosens. Bioelectron.*, 2017, **94**, 388–393.
33 M. Li and P. R. Selvin, Luminescent polyaminocarboxylate chelates of terbium and europium: The effect of chelate structure, *J. Am. Chem. Soc.*, 1995, **117**, 8132–8138.
34 H. L. Tan, Y. Q. Zhang and Y. Chen, Detection of mercury ions (Hg^{2+}) in urine using a terbium chelate fluorescent probe, *Sens. Actuators, B*, 2011, **156**, 120–125.
35 L. J. Charbonnière, R. Ziessel, M. Montalti, L. Prodi, N. Zaccheroni, C. Boehme and G. Wipff, Luminescent lanthanide complexes of a bis-bipyridine-phosphine-oxide ligand as tools for anion detection, *J. Am. Chem. Soc.*, 2002, **124**, 7779–7788.
36 B. Song, G. L. Wang, M. Q. Tan and J. L. Yuan, A europium (iii) complex as an efficient singlet oxygen luminescence probe, *J. Am. Chem. Soc.*, 2006, **128**, 13442–13450.
37 Y. Chen, Y. M. Chi, H. M. Wen and Z. H. Lu, Sensitized luminescent terbium nanoparticles: preparation and time-resolved fluorescence sssay for DNA, *Anal. Chem.*, 2007, **79**, 960–965.
38 L. Vijay, V. Meenakshi, R. Richa, P. Kamaldeep and K. Subodh, FRET-based ratiometric detection of Hg^{2+} and biothiols using naphthalimide-rhodamine dyads, *Org. Biomol. Chem.*, 2012, **10**, 8076–8081.
39 E. S. Childress, C. A. Roberts, D. Y. Sherwood, C. L. M. LeGuyader and E. J. Harbron, Ratiometric fluorescence detection of mercury ions in water by conjugated polymer nanoparticles, *Anal. Chem.*, 2012, **84**, 1235–1239.
40 F. Y. Zheng, S. H. Guo, F. Zeng, J. Li and S. Z. Wu, Ratiometric fluorescent probe for alkaline phosphatase based on betaine-modified polyethylenimine via excimer/monomer conversion, *Anal. Chem.*, 2014, **86**, 9873–9879.
41 Z. G. Song, R. T. K. Kwok, E. G. Zhao, Z. K. He, Y. N. Hong, J. W. Y. Lam, B. Liu and B. Z. Tang, A ratiometric fluorescent probe based on ESIPT and AIE processes for alkaline phosphatase activity assay and visualization in living cells, *ACS Appl. Mater. Interfaces*, 2014, **6**, 17245–17254.
42 R. Nishiyabu, N. Hashimoto, T. Cho, K. Watanabe, T. Yasunaga, A. Endo, K. Kaneko, T. Niidome, M. Murata, C. Adachi, Y. Katayama, M. Hashizume and N. Kimizuka, Nanoparticles of adaptive supramolecular networks self-assembled from nucleotides and lanthanide ions, *J. Am. Chem. Soc.*, 2009, **131**, 2151–2158.
43 P. K.-L. Fu and C. Turro, Energy transfer from nucleic acids to Tb(iii): Selective emission enhancement by eingle DNA mismatches, *J. Am. Chem. Soc.*, 1999, **121**, 1–7.
44 Y. P. Wu, X. Liu, Q. H. Wu, J. Yi and G. L. Zhang, Carbon nanodots-based fluorescent turn-on sensor array for biothiols, *Anal. Chem.*, 2017, **89**, 7084–7089.
45 H. L. Tan, B. X. Liu and Y. Chen, Lanthanide coordination polymer nanoparticles for sensing of mercury(ii) by photo-induced electron transfer, *ACS Nano*, 2012, **6**, 10505–10511.
46 N. Gao, Y. F. Zhang, P. C. Huang, Z. H. Xiang, F. Y. Wu and L. Q. Mao, Perturbing tandem energy transfer in luminescent heterobinuclear lanthanide coordination polymer nanoparticles enables real-time monitoring of release of the anthrax biomarker from bacterial dpores, *Anal. Chem.*, 2018, **90**, 7004–7011.
47 F. Pu, E. G. Ju, J. S. Ren and X. G. Qu, Multiconfigurable logic gates based on fluorescence switching in adaptive coordination polymer nanoparticles, *Adv. Mater.*, 2014, **26**, 1111–1117.

 This journal is © The Royal Society of Chemistry 2021